2003

Seasonal and ENSO variability in global ocean phytoplankton chlorophyll derived from 4 years of SeaWiFS measurements

James A. Yoder
University of Rhode Island, jimyoder@uri.edu

Maureen A. Kennely
University of Rhode Island

Citation/Publisher Attribution

Yoder, J. A., and M. A. Kennelly, Seasonal and ENSO variability in global ocean phytoplankton chlorophyll derived from 4 years of SeaWiFS measurements, Global Biogeochem. Cycles, 17(4), 1112, doi:10.1029/2002GB001942, 2003.
Available at: http://dx.doi.org/10.1029/2002GB001942

Seasonal and ENSO variability in global ocean phytoplankton chlorophyll derived from 4 years of SeaWiFS measurements

Seasonal and ENSO variability in global ocean phytoplankton chlorophyll derived from 4 years of SeaWiFS measurements

James A. Yoder and Maureen A. Kennelly
Graduate School of Oceanography, University of Rhode Island, Narragansett, Rhode Island, USA

Received 9 June 2002; revised 6 August 2003; accepted 6 October 2003; published 10 December 2003.

[1] The 4-year, calibrated SeaWiFS data set provides a means to determine seasonal and other sources of phytoplankton variability on global scales, which is an important component of the total variability associated with ocean biological and biogeochemical processes. We used empirical orthogonal function (EOF) analysis on a 4-year time series of global SeaWiFS chlorophyll *a* measurements to quantify the major seasonal (as well as the late El Niño and La Niña phase of the 1997–1998 ENSO) signals in phytoplankton biomass between 50°S and 50°N, and then a second analysis to quantify summer patterns at higher latitudes. Our results help place regional satellite chlorophyll variability within a global perspective. Among the effects we resolved are a 6-month phase shift in maximum chlorophyll *a* concentrations between subtropical (winter peaks) and subpolar (spring-summer peaks) waters, greater seasonal range at high latitudes in the Atlantic compared to the Pacific, an interesting phasing between spring and fall biomass peaks at high latitudes in both hemispheres, and the effects of the 1998 portion of the 1997–1998 ENSO cycle in the tropics. Our EOF results show that dominant seasonal and ENSO effects are captured in the first six of a possible 184 modes, which explain 67% of the total temporal variability associated with the global mean phytoplankton chlorophyll pattern in our smoothed data set. The results also show that the time (seasonal)/space (zonal) patterns between the ocean basins and between the hemispheres are similar, albeit with some key differences. Finally, the dominant global patterns are consistent with the results of ocean models of seasonal dynamics based on seasonal changes to the heating and cooling (stratification/destratification) cycles of the upper ocean. *INDEX TERMS:* 4227 Oceanography: General: Diurnal, seasonal, and annual cycles; 4215 Oceanography: General: Climate and interannual variability (3309); 4853 Oceanography: Biological and Chemical: Photosynthesis; 4275 Oceanography: General: Remote sensing and electromagnetic processes (0689); *KEYWORDS:* chlorophyll *a* concentrations, global, phytoplankton, SeaWiFS, variability

Citation: Yoder, J. A., and M. A. Kennelly, Seasonal and ENSO variability in global ocean phytoplankton chlorophyll derived from 4 years of SeaWiFS measurements, *Global Biogeochem. Cycles*, *17*(4), 1112, doi:10.1029/2002GB001942, 2003.

1. Introduction

[2] Seasonal to interannual changes in phytoplankton biomass and productivity are very important components of the total variability associated with ocean biological and biogeochemical processes. Phytoplankton are microscopic plants that are the principal photosynthetic organisms in the ocean and form the base of ocean food webs [*Falkowski and Raven*, 1997]. Chlorophyll *a* is the most important pigment involved in phytoplankton photosynthesis, and its concentration has been used as a proxy for phytoplankton biomass and photosynthetic potential for many decades [e.g., *Ryther and Yentsch*, 1957]. Ocean phytoplankton biomass (and thus chlorophyll *a* concentration) is highly variable in space and time. To a good first approximation, seasonal phytoplankton variability is related to stratification, destratification and incident solar irradiance [*Cushing*, 1959; *Longhurst*, 1998; *Dutkiewicz et al.*, 2001; *Gregg*, 2001]. The impact of these processes on phytoplankton growth and resulting biomass increase depends upon season and latitude. For example, wind mixing in the tropics (defined here as 10°N to 10°S) and subtropics (defined here as 10° to 40° north or south) [e.g., *Yoder et al.*, 1993; *Gregg*, 2001] can destratify the water column, bringing nutrient-rich waters to the surface where there is adequate solar irradiance for photosynthesis, thereby stimulating phytoplankton photosynthesis and growth. Conversely, strong and excessively deep mixing at high latitudes (defined here as >40° north or south) reduces mean photosynthetic irradiance of the mixed layer to below optimal levels for phytoplankton growth [*Sverdrup*, 1953; *Siegel et al.*, 2002]. At high latitudes, seasonal warming leads to a stratified water column which helps retain phytoplankton in well-lit and nutrient-rich surface waters, causing seasonal biomass peaks (blooms) [*Sverdrup*, 1953; *Riley et al.*, 1949]. However, strong stratification during summer at low latitudes

0886-6236/03/2002GB001942

and midlatitudes cuts off the supply of new nutrients to upper layers and often leads to low rates of photosynthesis and biomass [*Menzel and Ryther*, 1960; *Yoder et al.*, 1993]. Thus seasonal changes to physical forcing and the biological responses lead to seasonal changes in near-surface phytoplankton biomass (chlorophyll *a*) which differ depending on latitude, as well as other regional ocean characteristics.

[3] Beginning in the 1940s, oceanographers developed simple models to describe the important relations among mixing, stratification, solar irradiance, and nutrients, and how they interact to affect seasonal distributions of phytoplankton biomass and productivity [*Riley et al.*, 1949; *Steele*, 1974]. The links between physical processes and plankton production cycles quantified in those models originated from local and regional studies but are difficult to evaluate on global scales owing to lack of appropriate global plankton data sets. The Sea-Viewing Wide-Field Sensor (SeaWiFS), launched in fall 1997, provides a time series of phytoplankton chlorophyll *a* maps of the global ocean with unprecedented spatial and temporal coverage [*McClain et al.*, 1998; *Yoder et al.*, 2001]. Thus SeaWiFS can be used to globally evaluate various conceptual models linking physical and biological processes, at least at the level of phytoplankton biomass cycles. The purpose of this manuscript is to use a 4-year (1998–2001) time series of SeaWiFS chlorophyll *a* imagery to quantify the major seasonal signals in phytoplankton biomass, to determine interannual variability within the 4-year time series, and to find relations in the ocean-basin scale patterns.

2. Methods

[4] We chose to determine time and space patterns in the imagery using single value decomposition (SVD). SVD is a technique to calculate empirical orthogonal functions (EOF), and works best when applied to time series having no missing data (gap-free). Owing to cloud cover and other sampling problems, a gap-free time series of ocean chlorophyll imagery is impossible without considerable smoothing in time and space. Such smoothing will degrade the time and space resolution of features that can be resolved. For example, mesoscale features (such as ocean eddies) will not be resolved in the smoothed imagery we used for our analyses, nor we will fully resolve the effects of temporal phenomena (''events'') having characteristic timescales of days to weeks. Our focus, however, is on relatively large ocean features (> mesoscale) and on seasonal and longer timescales. To the extent possible with a 4-year time series, we also want some insight into interannual variability.

[5] Our basic data products were the global (9-km and 8-day resolution) SeaWiFS Version 3 chlorophyll *a* concentration images [*Hooker and McClain*, 2000] for the period January 1998 through December 2001, which we acquired from NASA's archive. These are image representations of binned data products. Using the maximum likelihood estimator (MLE) [*Campbell et al.*, 1995], which is similar to the geometric mean, to calculate the mean for each grid point, we calculated 0.25° × 0.25°, 8-day maps from the basic data product we obtained from NASA. We then smoothed the maps using 1° × 1° median box filter (with tapering) and then subsampled to 1° × 1° grid at 8-day resolution.

[6] As satellite chlorophyll data can be approximated with a lognormal distribution, we log-transformed the data and then used a three-point (24-day) running mean (and when necessary, used one of the three points to represent the mean) to smooth the time series in each pixel of our global grid. Between 50°N and 50°S, the globe at 1° × 1° resolution has 36,720 (360 × 102) possible grid points of which 28,071 are over the ocean. Our averaging and smoothing process resulted in a comparatively gap-free time series between 50°N and 50°S, with each of 19,484 ocean grid points having a 184-element time series (4-years with nominal 8-day resolution). An additional 6067 grid points were missing less than 5% of the data in the 184 element time series. We filled these missing values using the mean of four 8-day periods centered on the element of missing data. In no case did we use the mean fields to fill values missing more than three consecutive elements in the time series. With the exception of a few persistently cloudy or high aerosol regions (e.g., Arabian Sea), we had almost complete coverage of the ocean (91%) between 50°N and 50°S during each 8-day period.

[7] We wanted to resolve seasonal cycles, which can be more complex for plankton data than a simple annual cycle [*Longhurst*, 1998], and thus we chose to use simple data pre-treatment. We calculated, and then de-meaned the image time series by subtracting the 4-year temporal mean of each pixel (Figure 1b) from the pixel value in each of the 8-day maps. We also weighted each pixel value using the cosine of latitude (for equal area weighting). Our final array, A, consisted of 184 maps each comprised of 25,551 de-meaned, log (chl) values and weighted by cosine of latitude, i.e., A = [25,551, 184].

[8] We used the method of singular value decomposition (SVD) of the 4-year time series to calculate the temporal amplitudes, spatial eigenfunctions and corresponding eigenvalues [*Kelly*, 1988; *Yoder et al.*, 2002]. Since we first subtracted the 4-year temporal mean of each pixel (Figure 1b) from the corresponding pixel value in each of the 8-day maps before our calculations, the eigenfunctions of each mode are global maps of the average pixel deviations (with units of log chlorophyll *a* concentration) from the 4-year temporal mean shown in Figure 1b. We hereinafter refer to eigenfunctions as the ''spatial pattern for mode X'' or ''modal spatial pattern.'' The maps (matrices) are color coded and show both positive and negative deviations. The amplitude time series, a vector, associated with the spatial pattern of each mode is dimensionless and shows how the modal spatial pattern evolves with time. Thus all

Figure 1. (opposite) (a) Climatological CZCS mean chlorophyll and 4-year SeaWiFS chlorophyll (b) mean, (c) maximum, and (d) minimum images for 50°S to 50°N latitudes. The color bar applies to all frames, and the units are Log_{10} (chl *a*) + 2 (i.e., a log scale but with no negative numbers). The white region outside of land areas indicates insufficient data for EOF analyses (see section 2).

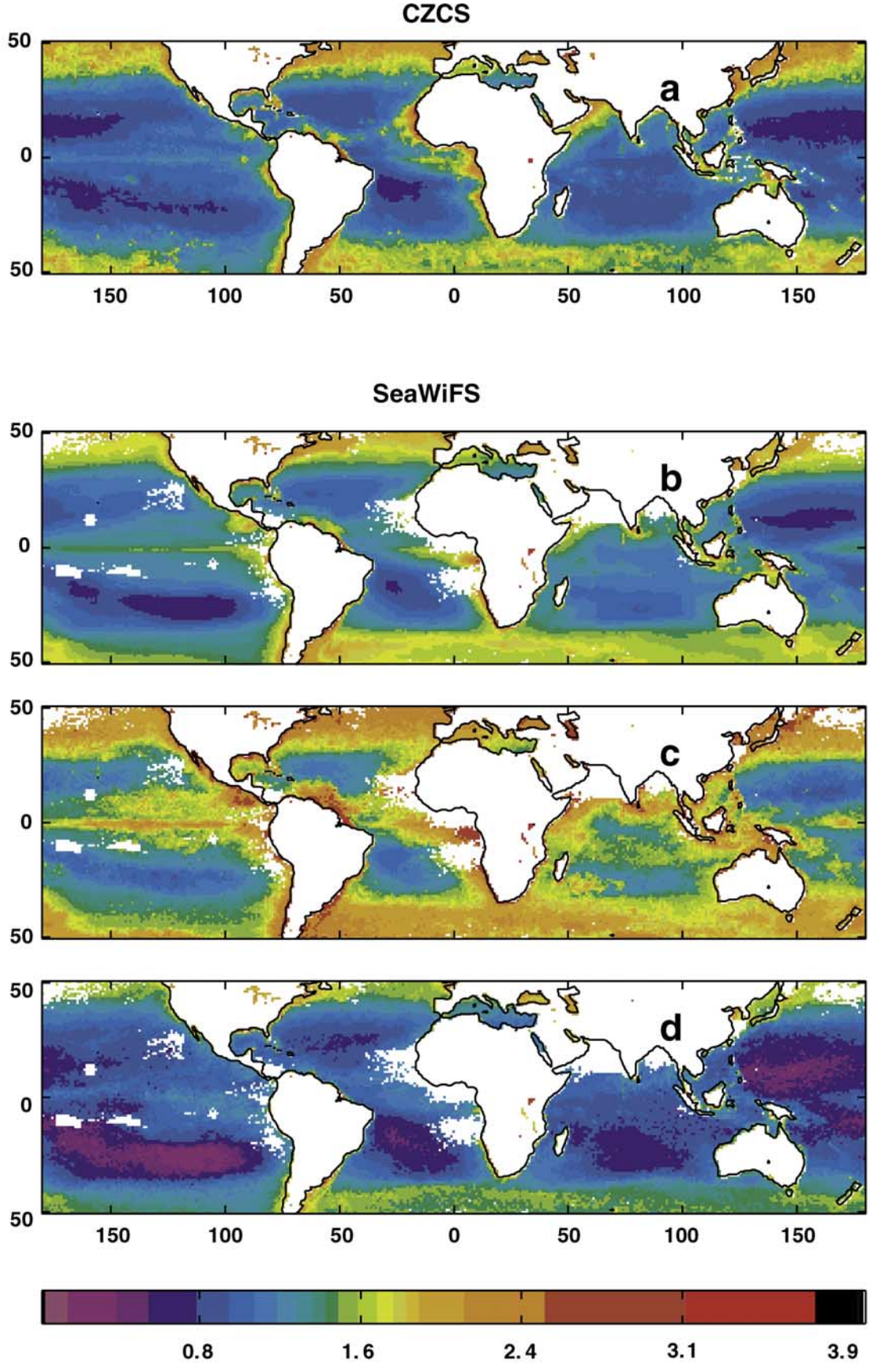
CZCS
a
SeaWiFS
b
c
d
50
0
50
150
100
50
0
50
100
150
0.8
1.6
2.4
3.1
3.9

pixels of a given modal spatial pattern change with time according to the single amplitude time series of that mode. SVD can be a very effective way to extract patterns from the large amount of data contained within image time series if: only a few modes (compared to the total length of the time series) account for most of the variability; the spatial patterns are relatively simple and coherent for large regions of the ocean; and the amplitude time series show smooth temporal patterns.

[9] In section 3, we focus on the dimensionless amplitude time series to describe temporal changes captured by each mode and the modal spatial pattern to identify regions of the ocean that are coherent. Since each mode has only one amplitude time series, areas of the global ocean where pixel values in the modal spatial pattern have similar values (and sign) have similar temporal deviations from the mean global pattern. Conversely, deviations from the mean global pattern are out of phase when pixels in the modal spatial pattern have similar values, but different signs. For any pixel at any point in the time series, chlorophyll deviations (in relation to Figure 1b) can be positive, negative, or zero as follows: (1) amplitude value and spatial pattern pixel value have the same sign yielding a positive chlorophyll deviation for that pixel and point in the time series from the mean pixel value in the global map (Figure 1b); (2) amplitude value and spatial pattern pixel value have different signs yielding a negative chlorophyll deviation for that pixel and point in the time series from the mean pixel value in the global map (Figure 1b); or (3) either the amplitude value or the spatial pattern pixel value are zero yielding no deviation from that pixel in the global map at that point in the time series.

[10] We estimated the sampling error of the eigenvalues and based on a 1-sigma criteria estimated that the first six modes (of 184 possible) were not degenerate [*North et al.*, 1982]. Here we focus on the first six modes, which represent 67% of the total variability, and for which we can relate to oceanographic processes. For each mode, we calculated and examined the homogeneous correlation coefficient using multiple linear regressions between the time series obtained at each pixel with the modal amplitude time series [*Wilson and Adamec*, 2001]. Maps of the correlation coefficient were used to help determine which pixels were the most closely related (and thus contributed most) to the mean modal amplitude time series [*Wilson and Adamec*, 2001]. Using standard methods, we also calculated and examined (but do not show) the communalities, which show how the variance accounted for by each mode changes throughout the time series. Plots of the communalities were particularly useful to distinguish ENSO.

[11] For the EOF analyses of complete annual cycles discussed above, we excluded results poleward of 50°N and 50°S owing to long data gaps during winter months caused by extensive cloud cover and low sun angles. We used a second analysis to focus on high-latitude (>50° north or south) growth seasons centered on the summer solstice in each hemisphere. As we wanted to cover complete growth seasons centered on the summer solstices with this second set of analyses, our first analyses of the Northern Hemisphere (NH) high-latitude growth season began in March 1998, and our first Southern Hemisphere (SH) growth season began in September 1998. The NH data set spanned the period from March 6 to September 29 (1998; 1999; 2000 and 2001), while the SH data set covered the interval from September 6 to March 29 (1998–1999; 1999–2000; 2000–2001 and 2001–2002). The resulting subsets consisted of 104 images (twenty-six 8-day intervals per year for 4 years) starting 80 days (ten 8-day intervals) after the winter solstice in each hemisphere. We included data collected from 15° to 80° N/S latitude, and focused on the first three modes. For these analyses we merged the results from 4 years into a single time series by ignoring the long gap of missing winter month data. Prior to the EOF analysis, we removed the 4-year temporal mean of each pixel from each of the 8-day maps and weighted each value using the cosine of latitude. We again used SVD to calculate the temporal amplitudes, spatial eigenfunctions, and corresponding eigenvalues. To determine the timing associated with the 1997–1998 ENSO cycle, we used the Nino 3.4 definition [*Trenberth*, 1997], which is calculated for the Pacific equatorial region encompassed by 5°N to 5°S and 170°W to 120°W. We obtained the index values from NOAA (http://www.cpc.ncep.noaa.gov/data/indices/index.html). Using this definition, the peak of El Niño was November 1997 (i.e., before our analyses) and the end was April 1998. The transition between El Niño and La Niña occurred between May and June 1998. La Niña started in July 1998, peaked in December 1998, and ended in February 2001. We used the *Hurrell et al.* [2003] definition of the North Atlantic Oscillation (NAO) index as obtained from the NCAR Climate Analysis Section web page, updated 2 June 2003 (http://www.cgd.ucar.edu/~jhurrell/nao.html).

3. Results and Discussion

3.1. Variability From 50°S to 50°N

[12] Figure 1 shows the 4-year mean global pattern of SeaWiFS-chlorophyll concentration from 50°S to 50°N and the 4-year maximum and minimum values, all on a log scale. The results in Figure 1 also show the mean global phytoplankton chlorophyll pattern as derived from all Coastal Zone Color Scanner observations (CZCS, Figure 1a). Both sensors agree qualitatively and show, for example, low chlorophyll concentrations in the ocean gyres, comparatively high concentrations in ocean margin waters and in the equatorial upwelling systems, and high mean concentrations within the ~40° to 50° N/S latitude belts (see *Gregg and Conkright* [2001] and *Gregg et al.* [2002] for quantitative analyses of the differences between CZCS and SeaWiFS global patterns). For SeaWiFS, note the persistence of the mean global pattern; that is, the same pattern is more or less evident in the mean, as well as maximum and minimum pixel values (Figures 1b, 1c, and 1d). The difference between maximum and minimum values is an estimate of the variability associated with the 4-year mean pattern. We used empirical orthogonal function (EOF) analyses to quantify some of the space-time characteristics of this variability.

[13] Figures 2 and 3 show the spatial patterns and associated amplitude time series (principal components)

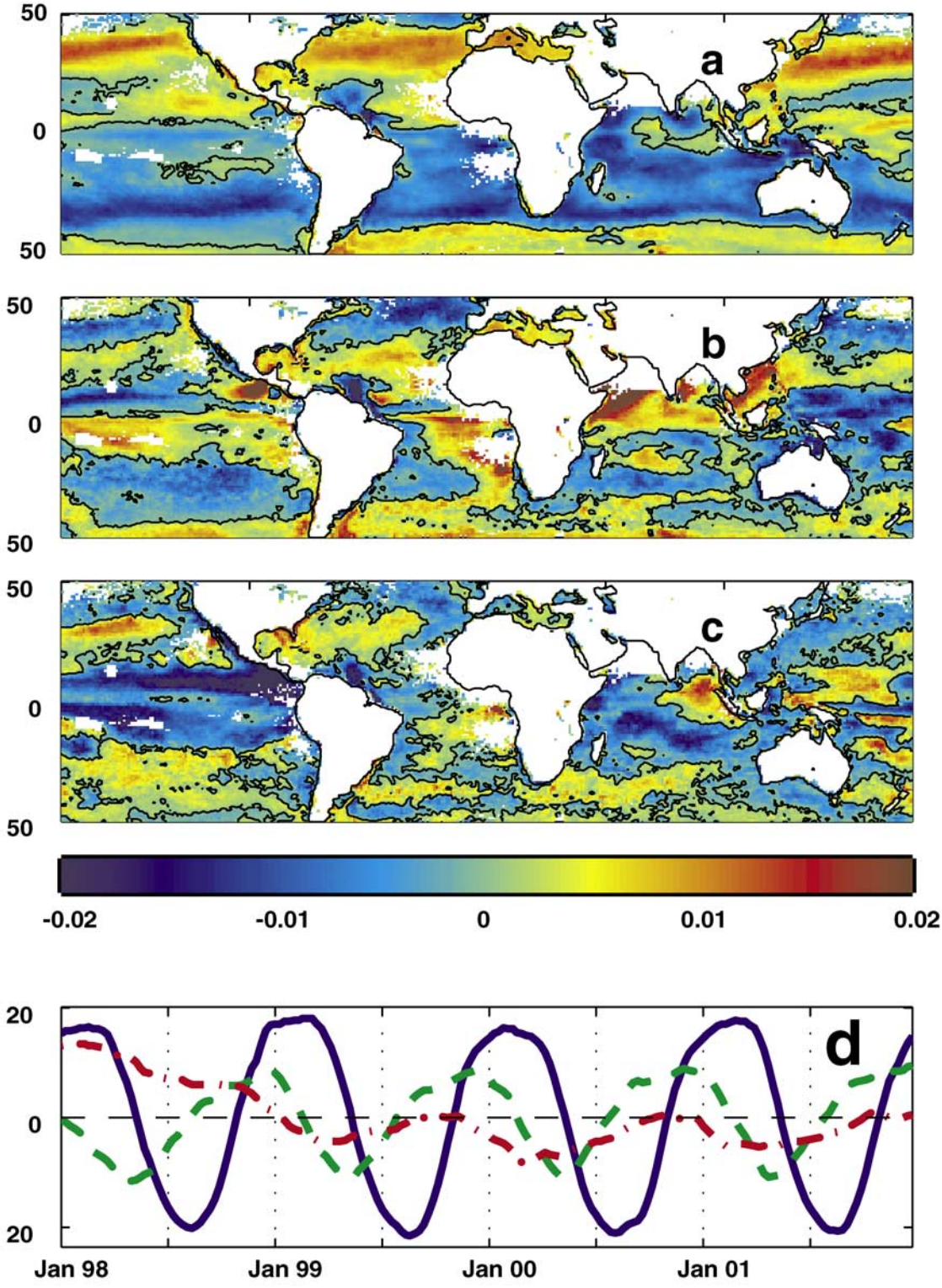

Figure 2. (a–c) Spatial patterns (50°S to 50°N) for modes 1–3 and (d) 4-year amplitude time series for modes 1–3. In Figure 2d, blue, green, and red lines correspond to modes 1, 2, and 3, respectively. Spatial patterns have units of Log_{10} (chl *a*), whereas amplitudes are dimensionless. As for Figure 1, the white region outside of land areas indicates insufficient data for EOF analyses (see section 2).

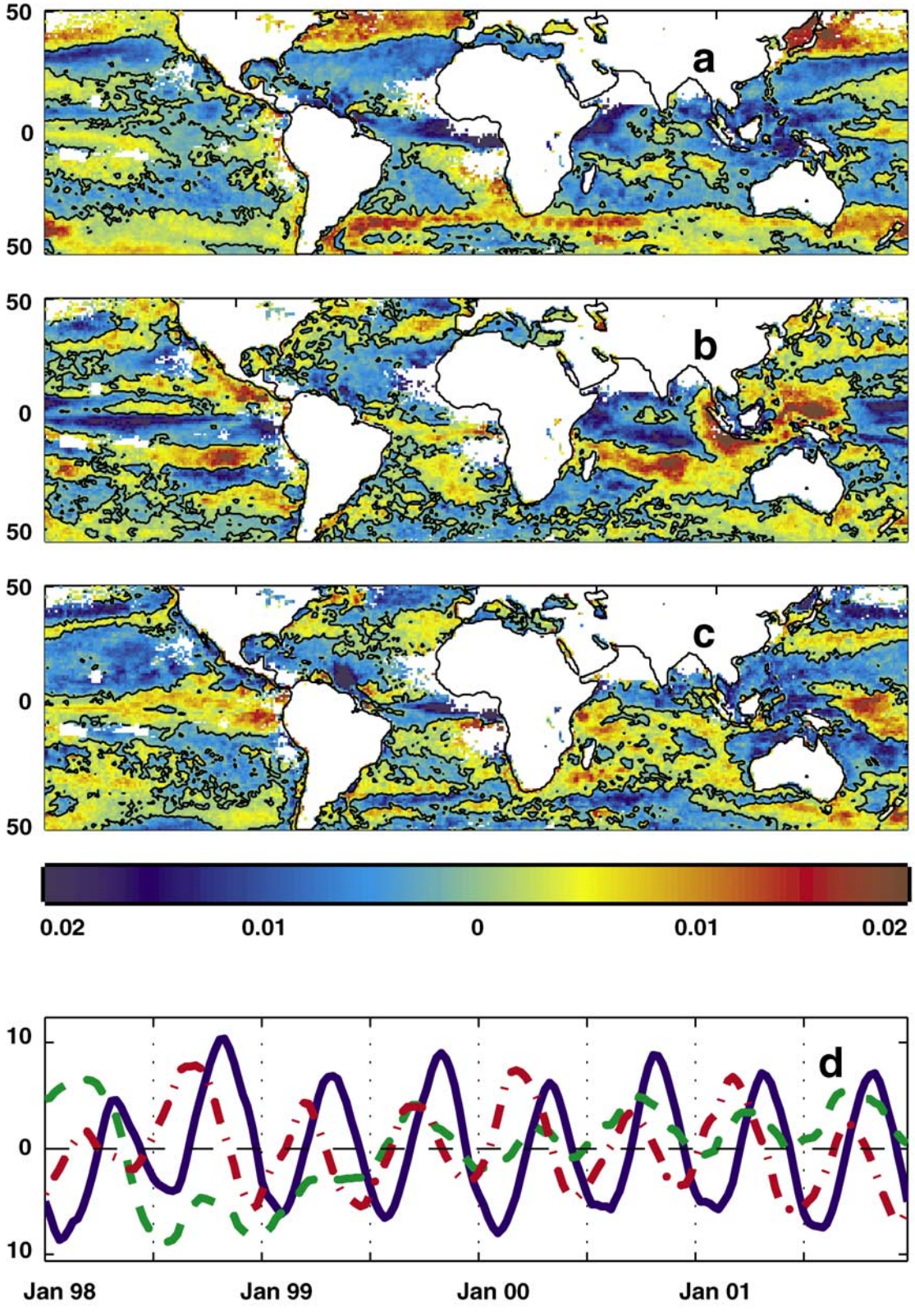

Figure 3. (a–c) Spatial patterns (50°S to 50°N) for modes 4–6 and (d) 4-year amplitude time series for modes 4–6. In Figure 3d, blue, green, and red lines correspond to modes 4, 5, and 6, respectively. Spatial patterns have units of Log_{10} (chl *a*), whereas amplitudes are dimensionless. As for Figure 1, the white region outside of land areas indicates insufficient data for EOF analyses (see section 2).

Table 1. Percent Variance Explained (PVE) for the First 8 Modes of the 50°N to 50°S Analyses

Mode	PVE, %	Cumulative PVE
1	41.	
2	9.1	50.1
3	6.1	56.2
4	5.2	61.4
5	3.3	64.7
6	2.7	67.4
7	2.0	69.4
8	1.8	71.2

for the first six modes of the EOF analyses, which account for 67% of the variability in the 4-year time series (Table 1). Some of the temporal patterns are well known from previous regional studies, and our results help put regional time/space variations within a global and multiyear context. Analyses of the global data also helps to establish linkages across and between ocean basins.

[14] Mode 1 (Figure 2a, and blue line in Figure 2d) accounts for 41.0% of the variability (Table 1) and is associated with dominant seasonal features. The amplitude time series is an approximate sine wave with peaks in either January or February (Figure 2d; Table 2) and troughs in August. The spatial pattern (Figure 2a) shows large areas of similar color-coded pixels indicating large-scale coherent structures within the ocean basins. As is evident by examining both the amplitude time series (Figure 2d) and the mean spatial pattern (Figure 2a) for the North Pacific and North Atlantic, mode 1 captures the 6-month phase shift between a winter maximum (positive deviations) and summer minimum (negative deviations) pattern at midlatitudes (~35°–45°N) versus the opposite pattern at high (>45°N) latitudes. As observed in previous studies of regional and global ocean color imagery [e.g., *Longhurst*, 1998; *Yoder et al.*, 1993, 2002], this phase shift is the main seasonal effect resolved by the first mode; the effect of the spring bloom is apparent in modes 2, 4, and 6.

[15] In the SH, the South Atlantic and Southern Indian have similar mode 1 responses as for the NH with the high-latitude pattern associated with the Sub-Antarctic Water Ring (south of 35°S) and the midlatitude pattern with the midlatitude gyre (~30°–35°S) [see *Moore and Abbott*, 2000]. The spatial pattern (Figure 2a) shows that positive deviations of midlatitude chlorophyll are oriented from southwest to northeast in both the North Atlantic and North Pacific, most evident from Figure 2a in the North Pacific.

[16] Regions that contribute the most to mode 1 temporal variability (i.e., highest homogeneous correlation coefficients) are the midlatitude regions (~30°–45°) of both hemispheres, the area just west of Indonesia, and the southwestern Indian Ocean. Mode 1 also reveals an asymmetric pattern in the NH tropical Atlantic. The spatial pattern of the western tropical Atlantic (Caribbean Sea) has predominantly negative pixel values (Figure 2a), whereas they are predominantly positive in the eastern tropical Atlantic. Thus the product of the negative summer values in the amplitude time series (Figure 2d) and the negative values in the spatial pattern in the tropical Atlantic (Figure 2a) yields positive summer chlorophyll deviations

Table 2. Timing of Minima and Maxima in the Annual Amplitude Time Series for Those Modes Showing Periodicities[a]

	Mode 1			Mode 2		
Year	Min/Max	Min/Max Int. Number	Date	Min/Max	Min/Max Int. Number	Date
1998	Max	7	18-Feb	Min	16	1-May
	Min	29	13-Aug	Max	45	19-Dec
1999	Max	8	26-Feb	Min	17	9-May
	Min	30	21-Aug	Max	45	19-Dec
2000	Max	4	25-Jan	Min	17	9-May
	Min	28	5-Aug	Max	43	3-Dec
2001	Max	8	26-Feb	Min	15	23-Apr
	Min	30	21-Aug	Max	46	27-Dec

	Mode 4			Mode 6		
Year	Min/Max	Min/Max Int. Number	Date	Min/Max	Min/Max Int. Number	Date
1998	Min	4	25-Jan	Max	10	14-Mar
	Max	16	1-May	Min	19	25-May
	Min	28	5-Aug	Max	33	14-Sep
	Max	39	1-Nov	Min	45	19-Dec
1999	Min	5	2-Feb	Max	10	14-Mar
	Max	16	1-May	Min	22	18-Jun
	Min	27	28-Jul	Max	32	6-Sep
	Max	39	1-Nov	Min	45	19-Dec
2000	Min	4	25-Jan	Max	9	6-Mar
	Max	16	1-May	Min	21	10-Jun
	Min	28	5-Aug	Max	33	14-Sep
	Max	39	1-Nov	Min	43	3-Dec
2001	Min	5	2-Feb	Max	9	6-Mar
	Max	16	1-May	Min	23	26-Jun
	Min	27	28-Jul	Max	33	14-Sep
	Max	39	1-Nov	Min	44	11-Dec

[a]"Int." refers to the 8-day compositing interval characteristic of SeaWiFS global data products.

in the east. Summer upwelling off the north coast of Venezuela and the effects of discharge from the Orinoco and Amazon Rivers are the likely explanations for the higher (in relation to the mean) chlorophyll concentrations [*Muller-Karger et al.*, 1989]. Finally, mode 1 shows a weak seasonal cycle (negative pixel values and thus positive summer deviations) associated with narrow upwelling regions centered on the equator in both the Atlantic and eastern Pacific. This seasonal feature (higher summer chlorophyll) is likely related to seasonal increase in the strength of the trade winds (and thus strength of upwelling) and was not well resolved by CZCS [*Halpern and Feldman*, 1994].

[17] Mode 2 (Figure 2b and green line in Figure 2d) accounts for 9.1% of the variability (Table 1). As for mode 1, the amplitude time series is also wave-like (Figure 2d) with peaks in December and troughs in April or May (Table 2). Mode 2 shows differences between the North Pacific and North Atlantic. The spatial pattern is strongly negative at higher latitudes in the North Atlantic, whereas there is a more complex pattern in the Pacific (Figure 2b). This difference is related to the more intense spring chlorophyll peak (i.e., negative pixels and negative values in the amplitude time series yield positive chlorophyll deviations) in the North Atlantic, compared to the North Pacific at comparable latitudes (>40°). Modes 1 and 2 spatial patterns both show a southwest to northeast oriented feature in the Atlantic and Pacific basins (reddish pixels in Figure 2a; bluish pixels in Figure 2b). Our results in the Pacific are consistent with a recent study [*Belkin et al.*, 2002] which showed that the mean orientation of the polar front was also southwest to northeast across the basin: near 40°N in the western Pacific and 50°–55°N in the eastern Pacific. Mode 2, in particular, shows positive deviations in late spring/early summer (product of negative amplitude values and negative spatial pattern pixel values) suggesting a spring bloom feature that follows the orientation of the polar front. Such a relation is consistent with local stratification associated with surface fronts affecting timing and magnitude of seasonal plankton blooms at middle to high latitudes [*Pingree et al.*, 1978].

[18] Mode 2 also shows a consistent high-latitude pattern throughout the Southern Ocean with generally positive spring-summer (September–February) deviations (positive amplitude values and spatial pattern pixel values) at latitudes higher than 40°S (Figures 2b and 2d). Also note that the mode 2 amplitude for January 1998 (during the 1997–1998 El Niño) is slightly negative, whereas it is strongly positive during January 1999–2001. Mode 2 also shows positive chlorophyll deviations in the subtropical waters (~10°–40°) during winter, particularly in the NH, as evidenced by the January peak (except for 1998) in the amplitude time series (green line in 2d) and the generally positive pixels values in the NH subtropics in the spatial pattern (Figure 2b). The subtropical pattern is caused by destratification during winter enhancing nutrient fluxes to surface waters in the subtropics where, in contrast to subpolar waters farther north, there is sufficient incident solar irradiance during winter for phytoplankton growth [e.g., *Cushing*, 1959; *Yoder et al.*, 1993; *Follows and Dutkiewicz*, 2002].

[19] Mode 3 (Figure 2c and red line in Figure 2d) and mode 5 (Figure 3b and green line in Figure 3d) show important 1998 ENSO effects. Mode 3 captures the ENSO effects in 1998 (end of El Niño, transition from El Niño to La Niña and beginning of La Niña) as evidenced by the amplitude time series (Figure 2d, red line), which is very different in 1998 than in the other 3 years (also see section 3.2). The mode 3 (and 5) amplitude time series are also different than those for modes 1, 2, 4, and 6. Furthermore, communalities showed that mode 3 contributes most to the total variance during the first half of 1998. A previous study [*Wilson and Adamec*, 2001] using EOF analyses of SeaWiFS chlorophyll and satellite-derived sea surface height anomalies in the equatorial Pacific between 30°S and 30°N concluded that the dominant biological response was a symmetric off-equatorial increase in chlorophyll (positive chlorophyll deviations from their mean pattern) between 2° and 18° during the transition from El Niño to La Niña ENSO phases (January–July 1998). The increase was attributed to increased nutrient supply owing to a shoaling thermocline. Our analyses of global imagery did not resolve this effect as clearly as for the previous study (which was focused on the equatorial regions), although it is captured to some extent in both modes 3 and 5 of our results. For example, the effect reported by *Wilson and Adamec* [2001] appears in our mode 5 as the change from positive amplitude values during the end of El Niño in first few months of 1998 (green line in Figure 3d) to negative values by the beginning of La Niña in July 1998. The predominantly positive pixel values in the mode 5 spatial pattern of the off-equatorial Pacific (Figure 3b), coupled with the aforementioned change in amplitude values, yield negative chlorophyll deviations for this region in the first few months of 1998 and higher deviations in July.

[20] Although partially obscured by persistent cloud cover in our results (Figure 2c and 3b), note the positive pixel values in the spatial pattern of modes 3 and 5 (Figures 2c and 3b, respectively) in the eastern tropical Atlantic south of the equator. As mode 3 and 5 amplitude time series values during the first 3–6 months of 1998 are also positive (Figures 2d and 3d), both modes show positive chlorophyll deviations. A previous study [*Signorini et al.*, 1999] concluded that enhanced chlorophyll concentrations in this region during El Niño were caused by enhanced river runoff. Mode 3 also shows a large area of positive pixel values (Figure 2c) for the eastern Indian Ocean off Indonesia. High chlorophyll concentrations there during El Niño may be caused by increased upwelling induced by abnormally high wind stress [*Gregg*, 2001]. Alternatively, smoke plumes from extensive Indonesian fires can confound processing of satellite imagery and lead to inaccurate and high satellite chlorophyll concentrations [*Murtugudde et al.*, 1999]. All fires had ceased by December 1997 [*Wooster and Strub*, 2002], i.e., at the peak of El Niño and before the start of our image time series. Thus the large area of positive mode 3 pixel values off Indonesia (Figure 2c), and thus positive chlorophyll anomalies during 1998, likely resulted from enhanced upwelling. Also note the large area of positive pixels in the Gulf of Mexico and western subtropical Atlantic during 1998 (Figure 2c). This may be related to unusually high El Niño-

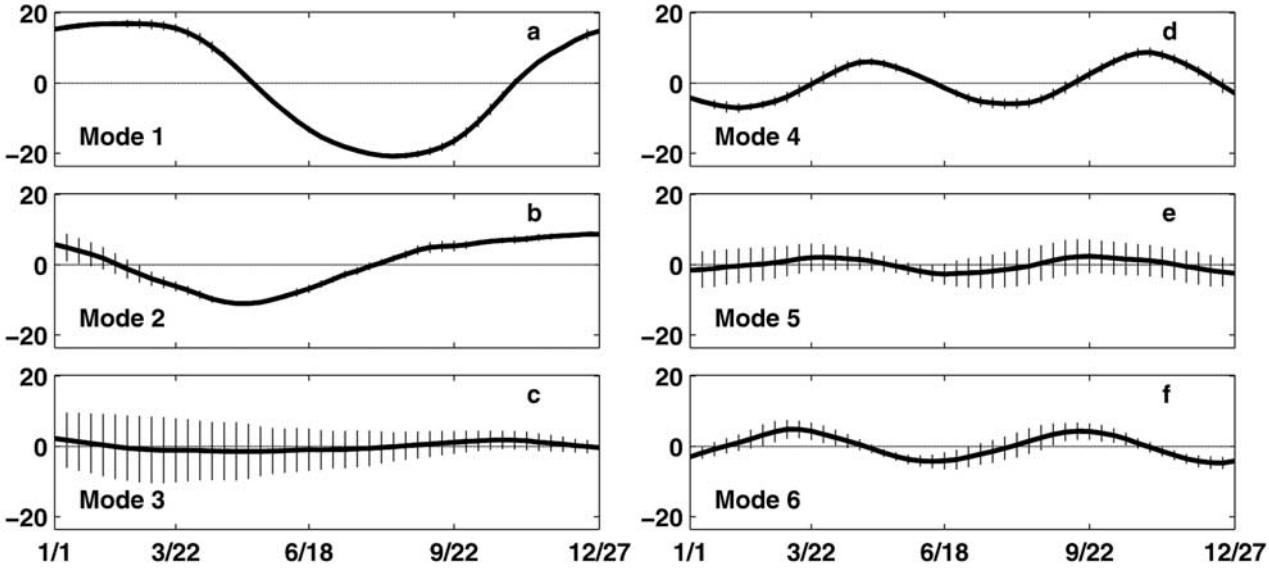

Figure 4. Four-year annual mean amplitude time series (dimensionless), and standard deviations (vertical line at each time interval), for modes 1–6. Also, see Table 2 for timing of the relative maxima and minima in modes 1, 2, 4, and 6.

related precipitation over the subtropical North Atlantic [*Smith et al.*, 1999] (Global Precipitation Climatology Project), as well as increased river discharge into the Gulf of Mexico and Atlantic, during the winter of 1997–1998. High precipitation and river discharge can increase nutrient flux to surface waters, leading to increases in phytoplankton biomass [*Muller-Karger et al.*, 1989].

[21] The amplitude time series of modes 4 and 6 (5.2 and 2.7 PVE, respectively: Table 1) are similar and represent an important modification of the mode 1 and 2 seasonal patterns. Note that the amplitude time series for both modes 4 (blue line in Figure 3d) and 6 (red line in Figure 3d) are wavelike, with two peaks and troughs per year: peaks in the NH spring (SH fall) and fall (SH spring) and troughs in the NH winter (SH summer) and NH summer (SH winter) (Figure 3d; Table 2). The 4 years are similar, although the minimum mode 4 amplitude occurs in January 1998, while mode 6 exhibits a maximum in the summer of 1998 (Table 2). The most interesting characteristic of modes 4 and 6 is that, with the exception of parts of the South Atlantic, the spatial pattern at latitudes poleward of about 25° is similar in both hemispheres (Figures 3a and 3c), although the seasons in the two hemispheres are 6 months out of phase. The reason for this symmetry is that the spring peak and summer minima in the NH coincide with the fall peak and winter minima in the SH and visa versa. This is consistent with a conceptual model proposed by *Cushing* [1959] and observed previously in CZCS imagery [*Yoder et al.*, 1993]. In brief, the spring peak at high latitude follows seasonal stratification and shoaling of the mixed layer above the critical depth [e.g., *Siegel et al.*, 2002]. The summer trough occurs in response to phytoplankton losses (grazing and sinking), and because nutrients are depleted in the strongly stratified mixed layer. The fall peak occurs in response to increasing wind stress, which begins to destratify the mixed layer and replenish nutrients resident below the seasonal thermocline. The winter trough at high latitudes occurs owing to low incident solar irradiance and deep mixed layers, which causes the mixed layer to be below the critical depth.

3.2. Interannual Variability in the Global Seasonal Patterns

[22] As discussed previously, interannual variability dominates mode 3 and based on its amplitude time series, spatial pattern, and a plot of communalities, that variability is most evident during the first part of 1998, i.e., during the El Niño and transition to the La Niña condition of the ENSO cycle. Some additional interannual variability is also evident in the seasonal patterns captured by modes 2, 5, and 6 (Figure 4). Figure 4 shows the 4-year mean and standard deviation of the amplitude time series for each of the first 6 modes. Modes 1 and 2 have very little variability in the amplitude time series (very small standard deviations) indicating very low interannual variability in the winter-summer phase shift between subtropical and subpolar waters in the global ocean (mode 1), as well as the primary spring-fall bloom pattern of subpolar waters (mode 2).

[23] Table 2 shows the timing of the minima and maxima associated with the four amplitude time series having strong seasonal patterns (modes 1, 2, 4, and 6). With only two exceptions, the relative minima and maxima of the amplitude time series for any given year did not differ from at least one of the other 3 years by more than one 8-day time-averaging interval. The two exceptions were the timing of the maxima of mode 2 in 2000 and the timing of the first minima of mode 6 in 1998.

[24] In addition to the timing of seasonal maxima and minima, the magnitude at the annual (or semiannual) peaks and troughs may also differ. For modes 1 and 2, variability of the amplitude at the seasonal maxima and minima was very small. The standard deviation of the amplitude of either the seasonal maximum or minimum varied by only 2.9 to 6.3%

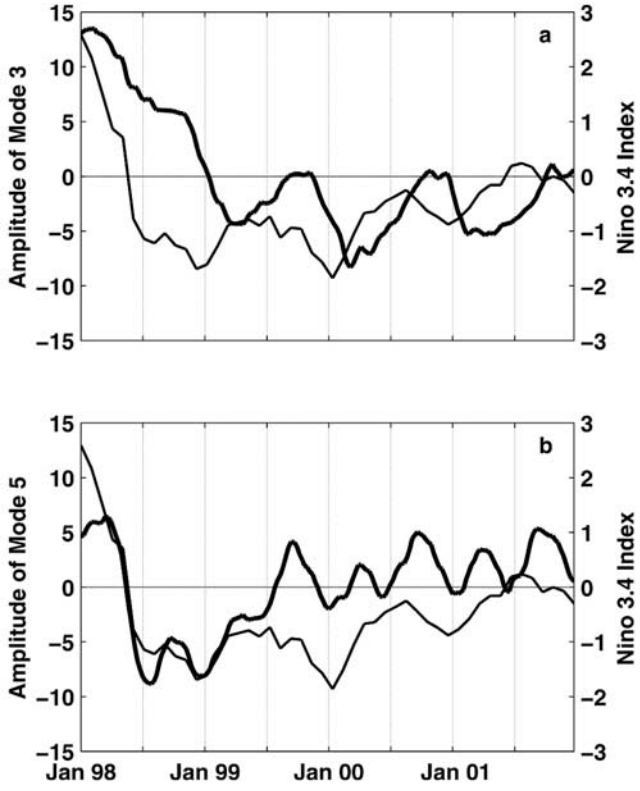

Figure 5. Four-year (a) mode 3 and (b) mode 5 amplitude time series (thick lines and left *Y* axes) and the Niño 3.4 index (thin lines and right axes).

of the 4-year maxima or minima mean value (Figure 4). There was more variability in amplitudes of the dual maxima and minima for mode 4 and more so for mode 6. For mode 4, standard deviations of the value for either the first or second maxima or minima (Table 2) ranged from 15 to 25% of the respective mean values, and by 36 to 56% for mode 6.

[25] For the modes showing the most interannual variability (modes 3 and 5, as well as the seasonal patterns of mode 6), the amplitude time series for year 1998 was the most different of the four (i.e., difference between the 1998 pattern from that of the other 3 years contributed the most to the standard deviations shown in Figure 4). From a plot of the communalities (not shown), mode 3 had its largest impact on total variance during the first half of 1998, whereas mode 6 had its largest impact during the second half of 1998.

[26] Figure 5 shows the Niño 3.4 index time series plotted with the mode 3 and 5 amplitude time series (Figures 5a and 5b, respectively), i.e., the two modes of the first six that show the most interannual variability. For mode 3 (Figure 5a), major features in the two time series are similar during the 4-year period with the amplitude time series lagging the index by $\sim$3–8 months. For mode 5, the index and the amplitude time series are closely related during 1998 and then diverge. These results are consistent with ENSO being the primary source of the interannual variability we observed in the global imagery used in our study.

[27] A previous study suggests that enhanced winter mixing of subtropical waters and associated increased nutrient flux to surface waters, a key characteristic of the negative state of the North Atlantic Oscillation (NAO), is an important source of interannual phytoplankton biomass and productivity variability (both higher than mean conditions) in the North Atlantic [*Follows and Dutkiewicz*, 2002]. SeaWiFS sampled two consecutive years (2000 and 2001) having very different NAO winter indices (2.80 and −1.89 as shown on the 2 June 2003 update on the Hurrell web page; see section 2). Values in the amplitude time series for modes 1 and 2 in the global data set are very similar for these 2 years (Figure 2d). Table 2 shows that the timing of the mode 1 peak is about 1 month later in 2001 than in 2000, but is similar to the timing of the peaks in 1998 and 1999, both of which had positive Hurrell NAO winter indices (0.72 and 1.7, respectively). Thus, unlike the association we show between the Niño 3.4 index and equatorial chlorophyll deviations, any North Atlantic chlorophyll deviations associated with ocean conditions indexed by interannual changes in the Hurrell NAO index, at least those observed in 2001 and 2001, were not evident in the first six modes of our analyses of global imagery. It is important to note that the global analyses include the tropics, which are strongly influenced by the ENSO signal that potentially masks other weaker interannual signals in the global imagery (see section 3.3).

3.3. Variability at High Latitudes

[28] For our second set of analyses which focused on high latitudes, particularly above 50°N/S, the first three modes explained 64% of the variance in the Northern Hemisphere and 61% in the Southern Hemisphere (Figures 6 and 7). Although the imagery did not provide complete seasonal coverage, the wave-like patterns of the mode 1 (48.5% PVE) amplitude time series for both NH and SH results (Figures 7a and 7d) clearly shows the 6-month phase shift between the middle and high latitudes also resolved in the previous analyses (i.e., midlatitudes have a winter maximum and high latitudes have summer maximum). The transition between these two regimes occurs near 50°N in the Atlantic and a few degrees farther south in the Pacific. All four years generally showed similar temporal patterns, although note the somewhat higher interannual variability in the spring. Figure 8 expands this part of the time series and shows that the spring of 2001 differs from the other 3 years in that the amplitude time series has a later and larger peak. This result from analyses focused on high latitudes is different than that previously described for the global analyses (50°N to 50°S), probably because tropical waters, which are strongly affected by ENSO, were excluded, thereby allowing weaker (than ENSO) interannual effects to be detected. The larger peak in spring 2001, when combined with the positive pixel values shown in Figure 6a, yields greater positive chlorophyll deviations (higher concentrations) in the subtropical waters of the North Atlantic (negative state of the NAO) compared to the other three springs (positive NAO). This is evidence suggesting that the effects of the oceanographic conditions associated with the NAO index are detectable as interannual chlorophyll anomalies in analyses focused on the NH.

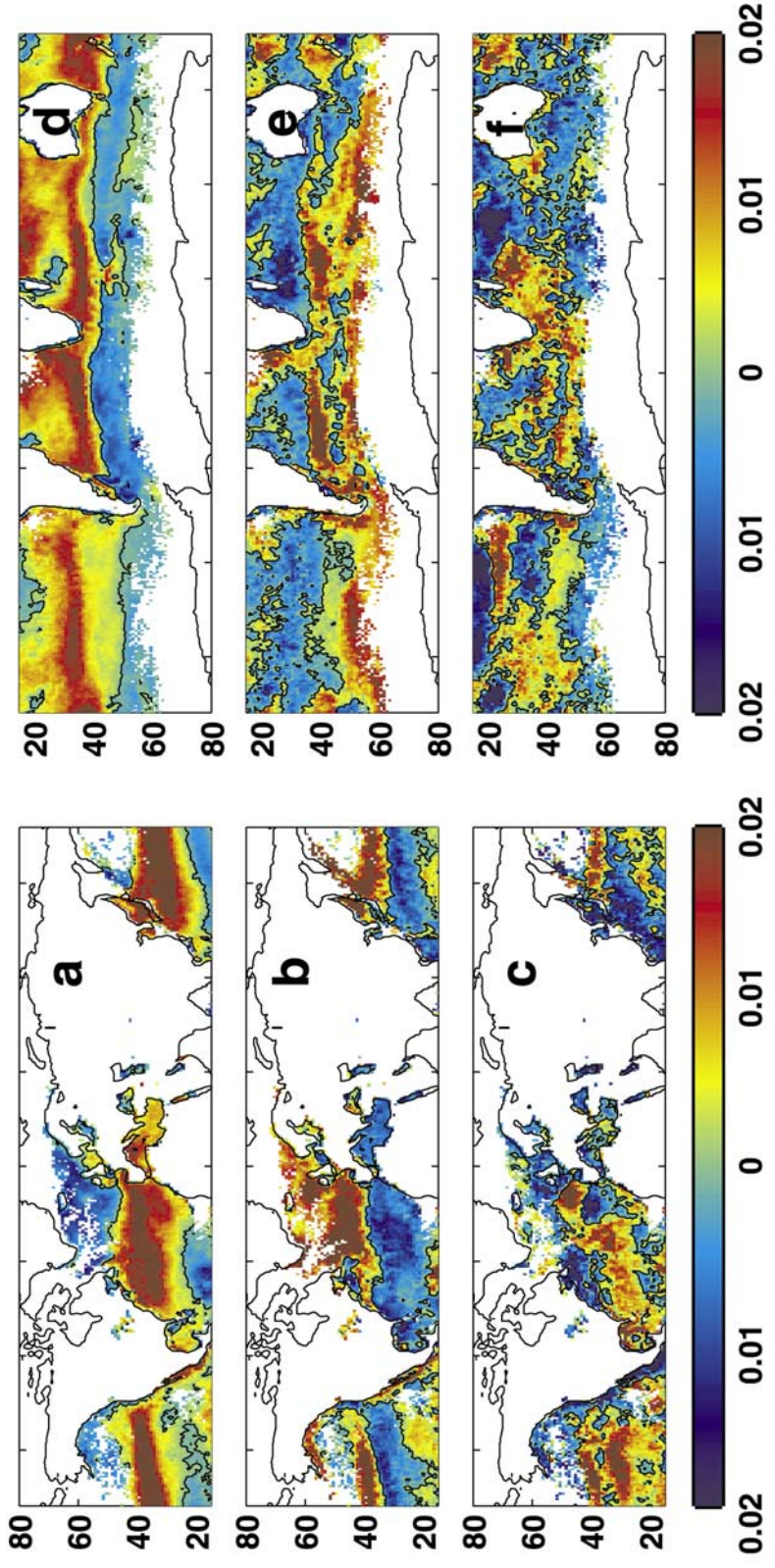

Figure 6. Spatial pattern (15° to 80°) for modes 1, 2, and 3 for high-latitude (a–c) NH and (d–f) SH. NH results spanned the period from March 6 to September 29 for 1998, 1999, 2000, and 2001, while SH results covered the interval from September 6 to March 29 for 1998–1999, 1999–2000, 2000–2001, and 2001–2002.

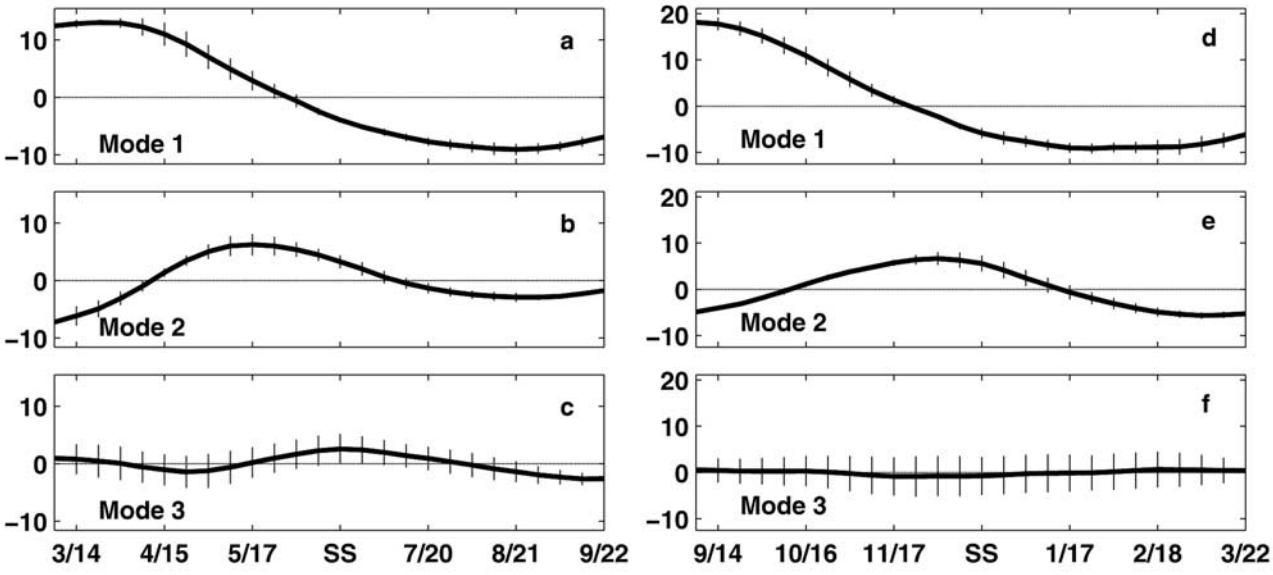

Figure 7. Four-year mean amplitude time series (dimensionless, centered on the summer solstice in the respective hemispheres) and standard deviation for modes 1, 2, and 3 for high-latitude (a–c) NH and (d–f) SH. NH results spanned the period from March 6 to September 29 for 1998, 1999, 2000, and 2001, while SH results covered the interval from September 6 to March 29 for 1998–1999, 1999–2000, 2000–2001, and 2001–2002.

[29] Mode 2 (10.8% of PVE) modifies the winter-summer pattern of mode 1 to enhance spring and lower winter chlorophyll deviations at latitudes north of ~40°N in the Atlantic (Figures 6b and 7b). The pattern is more complex in the Pacific with a latitude band between ~45°N and 50°N showing the opposite pattern from the Atlantic (i.e., Figure 6b shows negative pixels in the spatial pattern at that latitude band in the Pacific versus strongly positive pixels in the Atlantic). In the NH (Figure 6c) the coherent patterns associated with mode 3 (4.3% PVE, Figure 6c) are primarily south of 40°N and thus were better covered by the previous analyses.

[30] In general, SH modes 1 (46.3% PVE, Figures 6d and 7d) and 2 (9.5%, Figures 6e and 7e) are similar to comparable NH modes and thus are interpreted similarly. However, the peak in the SH mode 2 amplitude time series occurs about 1–2 months after (in relation to the summer solstice in the respective hemispheres) the NH peak (compare Figure 7b with Figure 7e). Both effects are related to the timing of the spring/summer blooms at high latitudes, which in the NH is directly related to increased mean irradiance of the water column [*Siegel et al.*, 2002]. Frontal features are more prevalent (and more important to phytoplankton biomass distributions) in the SH than in the NH [*Moore and Abbott*, 2000]. For example, high homogeneous correlation for mode 2 in a band at approximately 40°S in the Atlantic and Indian Oceans coincided with the position of the South Subtropical Front (SSTF). As for the NH, the mode 3 (5% PVE, Figure 6f) spatial pattern is quite complex, and the amplitude time series are nearly flat for all years, indicating poor resolution of any seasonal patterns. However, the mode 3 amplitude time series from the 4 years have higher standard deviations than the first two modes, indicating interannual variability (Figure 7f). Positive amplitudes in the SH occur from September 1998 until March 1999, whereas the following 3 years are all negative values. This is the principal indicator of interannual variability in these second analyses. Thus the mode 3 amplitude time series is very different than the other 3 years during the ENSO year of 1998. No potential explanations for high-latitude SH ENSO effects are offered here.

4. Conclusions

[31] Our results show that most of the variability (more than 67%) within 8-day composite global images from the first 4 years of SeaWiFS chlorophyll imagery is contained in the first six (of 184 possible) modes, and the resulting time/space patterns are interpretable in relation to seasonal to interannual ocean processes. The time and space smoothing that we used removed the effects of mesoscale (e.g., ocean eddies) and event (2- to 14-day) timescale phenomena, and thus it is not surprising that the first few modes are dominated by seasonal rather than higher frequency features. There is considerable variability at the seasonal and ENSO temporal scales, although a major feature of SeaWiFS data is that the mean global spatial (near-surface) chlorophyll pattern is very persistent. By this we mean that one sees the basic global spatial pattern of high versus low chlorophyll concentration regions, regardless of whether one views maps of the 4-year mean, maximum, or minimum chlorophyll concentrations.

[32] Our two highest modes accounted for 50% of the total variability in the 4-year times series of global observations (50°S to 50°N) and represented the important seasonal patterns in global chlorophyll distributions. Specifically, the two modes were primarily associated with differences between seasonal phase shifts between maxima

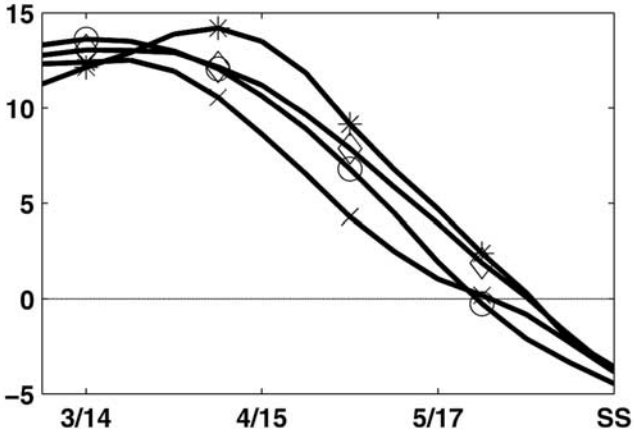

Figure 8. As for Figure 7, but only the mode 1 spring period (6 March to the summer solstice) for high-latitude NH is depicted to highlight interannual differences (1998, crosses; 1999, circles; 2000, diamonds; and 2001, asterisks).

and minima of subtropical (~20° to 40° N/S) and subpolar waters >45°N/S; and with the spring bloom in subpolar waters. The patterns in these two modes were evident in both hemispheres and across ocean basins. Furthermore, there was little evidence of interannual variability in these two modes for the analyses focused on the global ocean between 50°S and 50°N. The persistence of the mean global pattern, the spatially coherent patterns in the first two modes, and the lack of interannual variability in the first two modes define a ''first-order'' global near-surface chlorophyll distribution at spatial scales larger than mesoscales and at timescales longer than ''events. An interesting higher order (modes 4 and 6) seasonal characteristic was the symmetry caused by coincidence in the timing of spring maxima and summer minima in one hemisphere with the fall maxima and winter minima in the other.

[33] Interannual variability associated with the 1997–1998 ENSO was particularly evident in modes 3 and 5 with the effect of the La Niña portion of the 1997–1998 ENSO very evident in mode 3. Ocean color signatures of the 1997–1998 ENSO event in the equatorial Pacific and elsewhere were previously studied [e.g., *Chavez et al.*, 1999; *Murtugudde et al.*, 1999; *Wilson and Adamec*, 2001], and the results show that the regional impact of the 1997–1998 ENSO was large and also affected global productivity [*Behrenfeld et al.*, 2001]. In our study of global imagery, the impact of ENSO in 1998 was well represented in modes 3 and 5, which together accounted for 9.4% of the total variability. As discussed above, interannual variability was not very evident in either the timing or the magnitude of mode 1 and 2 seasonal maxima and minima in the 50°S to 50°N data analyses. However, when we excluded the tropics (and their ENSO signal) and focused on the higher latitudes, we found evidence that NH subtropical waters had a later and more intense spring peak in 2001 than in the other 3 years. A previous study showed that enhanced winter mixing of subtropical waters and associated increased nutrient flux to surface waters (a key characteristic of the negative state of the NAO) is an important source of interannual phytoplankton biomass and productivity variability (both higher than mean conditions) in the North Atlantic [*Follows and Dutkiewicz*, 2002].

[34] About 30% of the variability in our 4-year global data set, which was smoothed in both time and space to remove much of the high-frequency (days to weeks) and mesoscale (10- to 100-km) variability, was not explained by simple patterns. Rather, higher modes showed complex time and space structures. Some of this complexity may be related to regime shifts [*Karl*, 1999], other climate anomalies, or to propagating features such as eddies [*McGillicuddy et al.*, 1998] or planetary waves [*Uz et al.*, 2001] not resolved in our analyses. Understanding all major sources of phytoplankton variability is necessary for effectively designing global observing programs related to ocean carbon, nitrogen, and other element cycles and for developing and testing global ecosystem models. Our results help place regional satellite chlorophyll variability within a global perspective and contribute toward a better understanding of how to focus field observations to study seasonal and some interannual sources of variability in global ocean chlorophyll and, by implication, variability in primary production and other autotrophic processes.

[35] **Acknowledgments.** We thank S. Schollaert and M. Uz for technical and other assistance and for discussions of the results, as well as two anonymous reviewers who provided extensive comments that greatly improved the manuscript. We also thank ORBIMAGE, and the SeaWiFS Project and Distributed Active Archive Center (DAAC) at NASA's Goddard Space Flight Center for providing the SeaWiFS imagery used in our analyses. Financial support was provided by the National Science Foundation, NASA and by the University of Rhode Island.

References

Behrenfeld, M. J., et al., Biospheric primary production during an ENSO transition, *Science*, *291*, 2594–2597, 2001.

Belkin, I., R. Krishfield, and S. Honjo, Decadal variability of the North Pacific Polar Front: Subsurface warming versus surface cooling, *Geophys. Res. Lett.*, *29*(9), 1351, doi:10.1029/2001GL013806, 2002.

Campbell, J. W., J. M. Blaisdell, and M. Darzi, Level-3 SeaWiFS data products: Spatial and temporal binning algorithms, *NASA Tech. Memo.*, *32*(104566), 1995.

Chavez, F. P., P. G. Strutton, G. E. Friederich, R. A. Feely, G. C. Feldman, D. G. Foley, and M. J. McPhaden, Biological and chemical response of the equatorial Pacific Ocean to the 1997–98 El Nino, *Science*, *286*, 2033–2220, 1999.

Cushing, D. H., The seasonal variation in oceanic production as a problem in population dynamics, *J. Cons. Cons. Int. Explor. Mer.*, *24*, 455–464, 1959.

Dutkiewicz, S., M. Follows, J. Marshall, and W. W. Gregg, Interannual variability of phytoplankton abundances in the North Atlantic, *Deep Sea Res., Part II*, *48*, 2323–2344, 2001.

Falkowski, P. G., and J. A. Raven, *Aquatic Photosynthesis*, Blackwell Sci., Malden, Mass., 1997.

Follows, M., and S. Dutkiewicz, Meteorological modulation of the North Atlantic spring bloom, *Deep Sea Res., Part II*, *49*, 321–344, 2002.

Gregg, W. W., Tracking the SeaWiFS record with a coupled physical/biogeochemical/radiative model of the global oceans, *Deep Sea Res., Part II*, *49*, 81–105, 2001.

Gregg, W. W., and M. E. Conkright, Global seasonal climatologies of ocean chlorophyll: Blending in situ and satellite data for the Coastal Zone Color Scanner era, *J. Geophys. Res.*, *106*, 2499–2515, 2001.

Gregg, W. W., M. E. Conkright, J. E. O'Reilly, F. S. Patt, M. H. Wang, J. A. Yoder, and N. W. Casey, NOAA-NASA Coastal Zone Color Scanner reanalysis effort, *Appl. Opt.*, *41*, 1615–1628, 2002.

Halpern, D., and G. C. Feldman, Annual and interannual variations of phytoplankton pigment concentration and upwelling along the Pacific equator, *J. Geophys. Res.*, *99*, 7347–7354, 1994.

Hooker, S., and C. McClain, The calibration and validation of SeaWiFS data, *Prog. Oceanogr.*, *45*, 427–465, 2000.

Hurrell, J. W., Y. Kushnir, G. Ottersen, and M. Visbeck, An overview of the North Atlantic Oscillation, in *The North Atlantic Oscillation: Climatic Significance and Environmental Impact*, *Geophys. Monogr. Ser.*, vol. 134, edited by J. W. Hurrell et al., pp. 1–36, AGU, Washington, D. C., 2003.

Karl, D. M., A sea of change: Biogeochemical variability in the North Pacific subtropical gyre, *Ecosystems*, *2*, 181–214, 1999.

Kelly, K. A., Comment on ''Empirical orthogonal function analysis of advanced very high resolution radiometer surface temperature patterns in Santa Barbara Channel" by G. S. E. Lagerloef and R. L. Bernstein, *J. Geophys. Res.*, *93*, 15,753–15,754, 1988.

Longhurst, A., *Ecological Geography of the Sea*, Academic, San Diego, Calif., 1998.

McClain, C. R., M. L. Cleave, G. C. Feldman, W. W. Gregg, S. B. Hooker, and N. Kuring, Science quality SeaWiFS data for global biosphere research, *Sea Technol.*, *39*, 10–16, 1998.

McGillicuddy, D. J., A. R. Robinson, D. A. Siegel, H. W. Jannasch, R. Johnson, T. D. Dickey, J. McNeil, A. F. Michaels, and A. H. Knap, Influence of mesoscale eddies on new production in the Sargasso Sea, *Nature*, *394*, 263–266, 1998.

Menzel, D. W., and J. H. Ryther, The annual cycle of primary production in the Sargasso Sea off Bermuda, *Deep Sea Res.*, *6*, 351–367, 1960.

Moore, J. K., and M. R. Abbott, Phytoplankton chlorophyll distributions and primary production in the Southern Ocean, *J. Geophys. Res.*, *105*, 28,700–28,722, 2000.

Muller-Karger, F. E., C. R. McClain, T. R. Fisher, W. E. Esaias, and R. Varela, Pigment distribution in the Caribbean Sea: Observations from space, *Prog. Oceanogr.*, *23*, 23–64, 1989.

Murtugudde, R. G., S. R. Signorini, J. R. Christian, A. J. Busalacchi, C. R. McClain, and J. Picaut, Ocean color variability of the tropical Indo-Pacific basin observed by SeaWiFS during 1997–1998, *J. Geophys. Res.*, *104*, 18,351–18,366, 1999.

North, G. R., T. L. Bell, R. F. Cahalan, and F. J. Moeng, Sampling errors in the estimation of empirical orthogonal functions, *Mon. Weather Rev.*, *110*, 699–706, 1982.

Pingree, R. D., P. M. Holligan, and G. T. Mardell, The effects of vertical stability on phytoplankton distributions in the summer on the northwest European Shelf, *Deep Sea Res.*, *25*, 1011–1028, 1978.

Riley, G. A., H. Stommel, and D. F. Bumpus, Quantitative ecology of the plankton of the Western North Atlantic, *Bull. Bing. Oceanogr. Coll.*, *12*, 1–169, 1949.

Ryther, J. H., and C. S. Yentsch, The estimation of phytoplankton production in the ocean from chlorophyll and light data, *Limnol. Oceanogr.*, *2*, 281–286, 1957.

Siegel, D. A., S. C. Doney, and J. A. Yoder, The North Atlantic spring phytoplankton bloom and Sverdrup's critical depth hypothesis, *Science*, *296*, 730–733, 2002.

Signorini, S. R., R. G. Murtugudde, C. R. McClain, J. R. Christian, J. Picaut, and A. J. Busalacchi, Biological and physical signatures in the tropical and subtropical Atlantic, *J. Geophys. Res.*, *104*, 18,367–18,382, 1999.

Smith, S. R., D. M. Legler, M. J. Remigio, and J. J. O'Brien, Comparison of 1997–98 U.S. temperature and precipitation anomalies to historical ENSO warm phases, *J. Clim.*, *12*, 3507–3515, 1999.

Steele, J. H., *The Structure of Marine Ecosystems*, Harvard Univ. Press, Cambridge, Mass., 1974.

Sverdrup, H. U., On conditions for the vernal blooming of phytoplankton, *J. Cons. Perman. Int. Explor. Mer.*, *18*, 287–295, 1953.

Trenberth, K. E., The definition of El Nino, *Bull. Am. Meteorol. Soc.*, *78*, 2771–2777, 1997.

Uz, B. M., J. A. Yoder, and V. Osychny, Pumping of nutrients to ocean surface waters by the action of propagating planetary waves, *Nature*, *409*, 597–600, 2001.

Wilson, C., and D. Adamec, Correlations between surface chlorophyll and sea surface height in the tropical Pacific during the 1997–1999 El Nino-Southern Oscillation event, *J. Geophys. Res.*, *106*, 31,175–31,188, 2001.

Wooster, M. J., and N. Strub, Study of the 1977 Borneo fires: Quantitative analysis using global area coverage (GAC) satellite data, *Global Biogeochem. Cycles*, *16*(1), 1009, doi:10.1029/2000GB001357, 2002.

Yoder, J. A., C. R. McClain, G. C. Feldman, and W. E. Esaias, Annual cycles of phytoplankton chlorophyll concentrations in the global ocean: A satellite view, *Global Biogeochem. Cycles*, *7*, 181–193, 1993.

Yoder, J. A., J. K. Moore, and R. N. Swift, Putting together the big picture: Remote- sensing observations of ocean color, *Oceanography*, *14*, 33–40, 2001.

Yoder, J. A., S. E. Schollaert, and J. E. O'Reilly, Climatological phytoplankton chlorophyll and sea-surface temperature patterns in continental shelf and slope waters off the northeast U.S. coast, *Limnol. Oceanogr.*, *47*, 672–682, 2002.

M. A. Kennelly and J. A. Yoder, Graduate School of Oceanography, University of Rhode Island, South Ferry Road, Narragansett, RI 02882, USA. (m.kennelly@gso.uri.edu; jyoder@gso.uri.edu)